Review of Polyhedral Distortions as Multi-Scale Minimization of the Electric Polarization and Their Correlations With Physical Properties

Article *in* Acta Crystallographica Section B Structural Science · March 2006

DOI: 10.1107/S0108768105037985 · Source: PubMed

1 author:

Abderrahim Benabbas
Université de Bouira
54 PUBLICATIONS **441** CITATIONS

SEE PROFILE

Acta Crystallographica Section B
Structural Science
ISSN 0108-7681

Review of polyhedral distortions as a multi-scale minimization of the electric polarization and their correlations with physical properties

Abderrahim Benabbas

LIME Laboratory, University of Jijel, BP 98 Ouled-Aissa, 18000 Jijel, Algeria

Correspondence e-mail: benabbas_am@yahoo.fr

Received 17 July 2005
Accepted 17 November 2005

The Jahn–Teller (JT) and non-Jahn–Teller polyhedral distortions are reviewed within the same context, based on a multi-scale minimization of the electric polarization by handling formal ionic valences and valence electron density. This model is applied to tetragonal distortions of octahedra, particularly in K_2NiF_4 structures with different formula types, along with doping. The predictions are always in good agreement with the observed data. In particular, the ferrodistortive order of JT distortions is obtained from formal charge polarizations, while the antiferrodistortive one is adopted when only the valence electron density is involved. The correlations between physical properties and octahedral elongations through the crystal structures on one side and chemical compositions on the other side are discussed according to this model for high-T_c cuprate superconductors and CMR manganites.

1. Introduction

The Jahn–Teller (JT) theorem (Jahn & Teller, 1937; Kanamori, 1960) states that a non-linear system in a degenerate electronic state will be unstable and will undergo distortion to form a system of lower symmetry, thereby partially removing the degeneracy. This situation particularly encompasses the octahedral coordination of transition metal ions having a degenerate electronic configuration related to partially filled d orbitals such as d^9, high-spin d^4 and low-spin d^7. In these cases, the degeneracy is generally removed by the tetragonal elongation of octahedra. Even though theoretically predicted, the inverse situation (splitting of the orbitals as a result of compression of the octahedron) was never observed for such cations. For a review and applications of the JT effect several references can be consulted (Reinen, 1979; Bersuker & Polinger, 1989; Kaplan & Vekhter, 1995; Bersuker, 1996, 2005; Falvello, 1997; Whangbo & Koo, 2002). In the last two decades, especially since the discoveries of the high-T_c superconductivity in the cuprates and the colossal magneto-resistance in the manganites, the JT effect has received remarkable interest and has been the subject of much research. In both cases the parent compounds, containing the JT active ions Cu^{2+} and Mn^{3+}, respectively, are generally antiferromagnetic and the corresponding properties are obtained by an appropriate doping. Although the resulting JT distortions are attenuated, it seems that the JT effect remains a key factor in the mechanism for the two phenomena. The basis of the JT theorem is a coupling between the electronic and the nuclear motions, leading to minima (wells) in the potential energy surfaces (PES) according to the vibronic modes of the polyhedral distortions. The JT effect is termed dynamic when k_BT is comparable to the energy barrier between these minima so

the polyhedron will fluctuate between the corresponding configurations; otherwise the JT effect is static. Furthermore, in the absence of cooperative coupling, the static geometry may also be distributed statistically over the allowed configurations. These two types of fluctuations give rise to similar behaviour in X-ray diffraction experiments, which show large anisotropic displacement factors for the ligands. In a framework of connecting polyhedra, cooperative couplings through the commom oxygen anion can impose relationships between the orientations of distortions. In the case of octahedra, two types of cooperative two-dimensional configurations can be adopted: the ferrodistortive order as in La_2CuO_4 where all the octahedra are elongated in the same direction or the antiferrodistortive one as in $KCuF_3$, and K_2CuF_4 characterized by alternating elongations through parallel planes. Recently Lufaso & Woodward (2004) have underlined the interplay between the cooperative JT distortions, octahedral tilting and cation ordering in double perovskites by invoking the bond-valence sum concept.

By reviewing the structural databases, one can note that the distortions take place even in the absence of orbital degeneracy, as shown by the bond lengths around the Cu cation in the oxychloride $Ca_2CuO_2Cl_2$ (Hiroi *et al.*, 1996), where the Cu—Cl distance of 2.737 Å is greater than the sum of the ionic radii. Moreover, the magnitudes of octahedral elongations can spread out over a wide range, as shown in the high-T_c cuprate superconductors, where the Cu—O apical bonds can attain 2.85 Å (Dai *et al.*, 1995), whereas the average distance is around 2.25–2.40 Å. These large differences in bond lengths show that the valence-electron distributions on the Cu cation are far from the simple image of one or two electrons per $d_{x^2-y^2}$ or d_{z^2} orbital. Charge-density research (Tsirelson & Ozerov, 1996; Tsirelson & Stash, 2004; Lecomte *et al.*, 2005) using accurate X-ray diffraction and multipole model fitting shows similar behaviour for other classes of materials. On the other hand, it is important to point out that not only pronounced octahedral elongations but also compressions are encountered with non-JT active cations such as Ni^{2+} as in La_2NiO_4 (Grande & Mueller-Buschbaum, 1977) and U^{6+} in Cs_2UO_4 (Kovba *et al.*, 1961). However, there is a distinction in the literature between the JT ions such as Cu^{2+}, Cr^{2+} and Mn^{3+} ions and the non-JT ones. On the other hand, a second-order Jahn–Teller (SOJT) effect is invoked for the off-centering of the small high-valent d^0 cations such as W^{6+}, Nb^{5+} and Ti^{4+} in their octahedra (Bader, 1960, 1962; Pearson, 1983; Wheeler *et al.*, 1986).

In this paper we will review such distortions without any distinctions and show that they are generated by the same process, reflecting a multi-scale minimization of the electric polarization. Their simple use in the first step of formal ionic valences and in the second step of the valence-electron distribution allows us to understand and predict the relative magnitudes and the directions of distortions. Practically, the octahedral elongations are found to deeply influence the physical properties of the corresponding structures. Their relationships are briefly discussed for the high-T_c cuprate superconductors and the manganites.

2. Background

Devonshire (1949, 1951, 1954) proposed a phenomenological theory of the ferroelectricity in $BaTiO_3$. He expressed the free energy as a function of the polarization components P_x, P_y and P_z. Structurally, Mason & Matthias (1948) associated this property with the off-center positions of the Ti^{4+} ions in their octahedra. In addition to the ionic polarization, Slater (1950) introduced electronic polarization.

The structure adopted by a solid corresponds to the minimum of the total energy, which includes (besides the kinetic part) different contributions from coulombic interactions such as the valence-electron mutual interactions, the interactions of valence electrons with the atom cores and those between the cores (Harrison, 1980). On the other hand, the bonds occurring in a charge distribution can be treated in terms of the density-difference distribution (Bader *et al.*, 1967; Bader, 1990).

The potential energy can be correlated to the electric polarizations or the electric dipoles associated with the charge distribution (charge positions). These polarizations relate to different scales (local polarizations) including the valence electrons, core shells and nuclei (Purcell & Ramsey, 1950; Rainwater, 1950). The structure adopted by a solid will correspond to the multi-scale minima of the electric polarization, which occurs from the minimization of local distances between opposite charges, leading to the minimization of the net charge associated with a more extented volume, and so on. This means that if a set of charges is put in a hypothetical configuration having a net polarization, these charges will undergo the effects of the mutual electric fields and move towards their equilibrium positions corresponding to the multi-scale minima of the polarization. If the polarization is considered with its underlying components, the multi-scale minimization will relate to the norm of the total polarization and of the components together. These minima result in spontaneous polarization for the ferroelectric materials, whereas the total polarization is null at the unit-cell level for paraelectrics. For example, in the tetragonal $PbTiO_3$ structure (Shirane *et al.*, 1956) the shift along z of 0.30 Å for the Ti^{4+} ion and the much larger shift of 0.47 Å in the same direction for the Pb^{2+} ion are essentially driven by the small size of the former. Its off-centering is imposed by the local minimization of the polarization; the subsequent excess negative charges at the mid-plane of the oxygen octahedron will displace the Pb^{2+} ion in the same direction (to also locally minimize the polarization) to an equilibrium position fixed especially by its size. The larger the ion in this site the shorter is its displacement, *i.e.* the local polarization is less attenuated and the resulting total polarization will be more pronounced, as shown by the structural data and the ferroelectric properties of $PbTiO_3$ and $BaTiO_3$. We can say that the ferroelectric properties of non-centrosymmetrical structures are related to the results of the local minimizations of the polarization and are generally favoured by large differences in the size of the constituent cations. The vibronic motions are considered to be perturbative effects that can, with increasing temperatures, modulate

the ionic sizes and induce a transition to a more symmetrical structure. We adopt in this paper a structural approach to explain and predict the octahedral distortions, particularly in bidimensional structures whose analysis is more direct and illustrative.

3. Application

The bidimensional Ruddlesden–Popper structures $A_{n+1}B_nO_{3n+1}$, in which n perovskite layers alternate with one rocksalt layer, are adopted by a great number of transition-metal-based oxides (B = Cu, Ni, Fe, Co, V, Ti, Nb *etc.*). Owing to its wide variety of structural features and related physical properties (Ganguly & Rao, 1984; Rao *et al.*, 1988), the K_2NiF_4 structure (Fig. 1), corresponding to $n = 1$, has received considerable interest, before and after the discovery of high-T_c superconductivity in $La_{2-x}Ba_xCuO_{4-\sigma}$ (Bednorz & Muller, 1986). The stability of this structure is commonly interpreted by geometric factors using the same tolerance factor t (Birgeneau *et al.*, 1970) defined for the perovskites as

$$t = (R_A + R_O)/2^{1/2}(R_B + R_O) \quad \text{with } t > 0.87,$$

where R_A, R_B and R_O are the ionic radii of the constituent elements corresponding to the general formula A_2BO_4, which somewhat reflects the size adaptability between perovskite and rocksalt layers. Consequently, as proposed by Singh *et al.* (1984), these layers should be under compressive and tensile stresses, respectively. In the xy plane, the $A-O$ bonds tend to be lengthened while the $B-O$ bonds tend to be shortened; on the contrary, the $B-O$ bonds along z are straightened out. One can, however, note that the efficient way to minimize the presumed tensile stress in the rock-salt layers should be realised by adjusting the positions of the A cation and the apical oxygen anion at the same level in the xy plane, which allows maximization of the layer size in this direction. In all cases where the octahedra are elongated, the A cation is always displaced along z, clearly below the apical oxygen anion. This structure can also be characterized by the c/a ratio of the cell parameters, which is equal to 3.41 for the ideal ionic structure. This ratio may sometimes indicate the magnitude of the tetragonal elongation of the BO_6 octahedra, but there is not always a direct correlation. Furthermore, Demazeau *et al.* (1984) argued that this elongation can be enhanced by increasing the covalency of the $B-O$ bonds in the xy plane. Since the $A-O$ bonds are generally less covalent than the $B-O$ bond (the A element being generally more electropositive), one can deduce that the competition in the xy plane ($B-O-B$) and along **z** ($A-O-B$) should in principle lead to an opposite effect, *i.e.* the compression of the octahedron. In this context it is noteworthy that none of these models has taken into account an important feature, namely the ionic valence states, at least the formal one; it is useful to note that the majority of the $A^{3+}B^{3+}O_3$ perovskites adopt the distorted orthorhombic $GdFeO_3$ structure (Geller & Wood, 1956; Roth, 1957), even if the geometric factors are favourable for a higher symmetry.

To illustrate our approach, we consider the well known and studied phase of La_2CuO_4 (Longo & Raccah, 1973), with the K_2NiF_4 structure. Owing to its layer structure, it will be treated as a juxtaposition, perpendicular to z, of successive layers: –(LaO)–(CuO_2)–(LaO)–(LaO)–(CuO_2)– (Fig. 2). To understand the structural configuration adopted by La_2CuO_4, we will artificially place the ions at the positions corresponding to the undistorted structure. The superposition principle allows us to handle these layers as uniform blocks. Their formal charges are deduced from the formal ionic charges of the

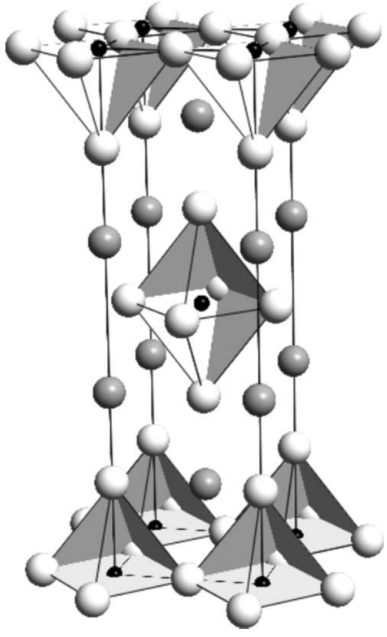

Figure 1
The K_2NiF_4 structure.

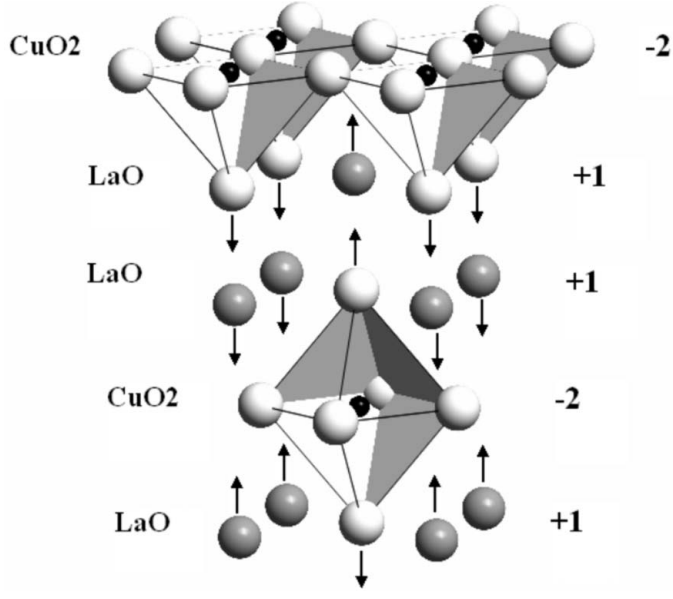

Figure 2
The formulae and the formal charges of the idealized layers and the ionic displacements in La_2CuO_4.

corresponding ions. In this case, the resulting charges per formula unit are, respectively, –(+1)–(−2)–(+1)–(+1)–(−2)–, reflecting interlayer polarizations. As a consequence of these polarizations, every layer will experience the electric field created, as a first approximation, by the neighbouring layers. In order to minimize these polarizations, the constituent ions will move along **z** in the direction imposed by the resulting electric field and the signs of their charges, until they reach their equilibrium (real) positions. Owing to the layer sequence, only the lanthanum cation and the apical oxygen anion in the rock-salt layers are affected: the former will move towards the CuO_2 layer and the latter in the opposite direction, which explains the tetragonal elongation of the CuO_6 octahedron observed and also the location of the La cation along **z**, below the apical oxygen anion. According to the presence of a mirror symmetry (at the CuO_2 layer), the total polarization is null. The same behaviour is encountered in the other isovalent $A_2^{3+}B^{2+}O_4$ compounds La_2NiO_4 (Grande & Mueller-Buschbaum, 1977) and Nd_2NiO_4 (Nishijima *et al.*, 1991) (Table 1). The differences in the magnitude of octahedral elongations can be interpreted by going beyond the spherical model of ions and the formal valence and taking into account the displacement of valence electrons away from the nagative BO_2 layer. Within the stability limits, this elongation decreases with the size of the A cation, since the interlayer polarizations will be less pronounced.

An analogous scheme is applied to other isotypic compounds, such as the two classes $A^{3+}A'^{2+}B^{3+}O_4$ and $A_2^{2+}B^{4+}O_4$. In the former, the formal charges of the corresponding layers are –(+0.5)–(−1)–(+0.5)–(+0.5)–(−1)–, which gives the expectation of an attenuation of the octahedral elongations with respect to $A_2^{3+}B^{2+}O_4$, which is in good agreement with the structural data of $NdSrMnO_4$ (Sander *et al.*, 1981), $LaSrFeO_4$ (Soubeyroux *et al.*, 1980), $LaSrCuO_4$ (Goodenough *et al.*, 1973), $LaSrVO_4$ (Greedan & Gong, 1992), $LaSrCoO_4$ (Demazeau *et al.*, 1979), $LaSrAlO_4$ (Shannon *et al.*, 1992) and $LaSrGaO_4$ (Britten et *al.*, 1995) (Table 2). The example of $LaSrCuO_4$ is important to be considered: the classical approach states that the ordering of the two holes on the $d_{x^2-y^2}$ orbital of the low-spin d^8 Cu^{3+} cation should in principle accentuate the octahedral elongation with respect to the d^9 Cu^{2+} cation, where only one hole is present.

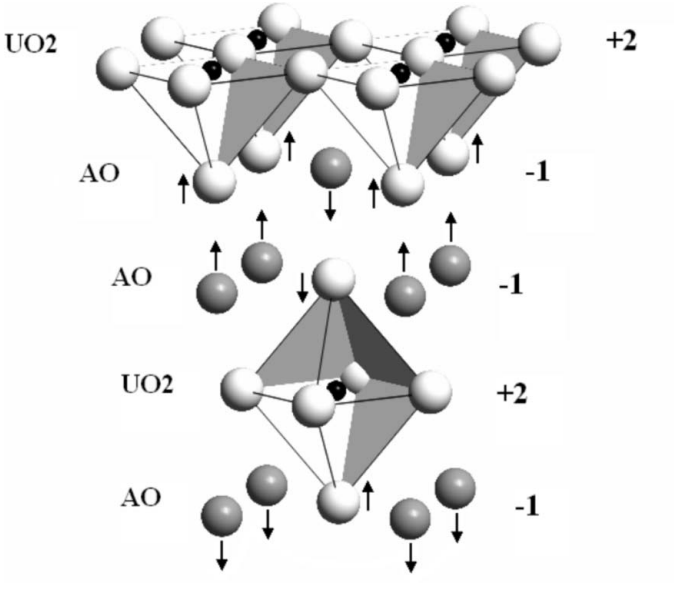

Figure 3
The formulae and the formal charges of the idealized layers and the ionic displacements in A_2UO_4.

Table 1
The $B-O$ bonds lengths in $A_2^{3+}B^{2+}O_4$ phases.

Phase	La_2CuO_4	La_2NiO_4	Nd_2NiO_4
d_{B-O} (Å)	1.90 × 4	1.938 × 4	1.927 × 4
	2.40 × 2	2.279 × 2	2.260 × 2

In the $A_2^{2+}B^{4+}O_4$ class, the formal charges of layers are neutral and thus the octahedral distortions are too small to be observed, as shown by Sr_2FeO_4 (Dann *et al.*, 1991), Sr_2TiO_4 (Lukaszewicz, 1959) and Sr_2VO_4 (Range *et al.*, 1991; Table 3). The weak magnitude and the direction of the distortion are related to the distribution of the valence-electron density around the core shell of ions. The neutral layers are also present in the structure of K_2CuF_4 (Khomskii & Kugel, 1973). The minimization of polarizations is attained by the antiferrodistortive order of elongated octahedra in the xy plane. This configuration reflects the maximum distances between the maxima of valence electron density around the Cu cation.

The intermediate phases $A_x^{3+}A_y'^{2+}BO_4$ ($x + y = 2$) are to be considered between the corresponding extreme cases. In particular, hole doping carried out on these phases always reduces the $B-O$ apical bond length in correlation with the reduction of the absolute formal charges of the layers. An important feature must be underlined: according to the formal charge, the octahedral elongation around the d^4 Mn^{3+} cation is therefore less pronounced than that around d^9 Cu^{2+}, while the octahedron of d^4 Fe^{4+} is nearly undistorted. The absence of distortions was also attributed to the delocalization of the e_g electron (Bocquet *et al.*, 1992; Takeda *et al.*, 1994).

Examples of the structures of the uranium oxides A_2UO_4 (A = K, Rb, Cs; Fig. 3) constitute another argument for this model. The formal charges of the layers are –(−1)–(+2)–(−1)–(−1)–(+2)–, so the displacements of the rocksalt ions are inverted and the UO_6 octahedra will be compressed, as shown by the structural data of these compounds (Kovba *et al.*, 1961) (Table 4).

The uranium oxides are classified into two subgroups, namely the uranates where the U—O distances are identical or nearly equal and the uranyls (most common) with two short axial U—O bonds associated and denoted as the UO_2^{2+} ion, and which is surrounded by a number of equatorial ligands at longer distances (Obbade *et al.*, 2003; Duribreux *et al.*, 2003; Sykora & Albrecht-Schmitt, 2004; Woodward *et al.*, 2004). In the uranyl structures, the axial U—O bonds generally point towards the alkali or alkaline-earth ions. These dispositions are analogous to that of A_2UO_4 and are at the origin of the shortening of these bonds. Furthermore, the decrease of these axial bonds with the Cs/U ratio in the related structures of

Table 2
The $B-O$ bond lengths in $A^{3+}A'^{2+}B^{3+}O_4$ phases.

Phase	$NdSrMnO_4$	$LaSrFeO_4$	$LaSrCuO_4$	$LaSrVO_4$	$LaSrCoO_4$	$LaSrAlO_4$	$LaSrGaO_4$
$d_{B\text{-}O}$ (Å)	1.888 × 4	1.942 × 4	1.88 × 4	1.941 × 4	1.912 × 4	1.878 × 4	1.922 × 4
	2.281 × 2	2.154 × 2	2.23 × 2	2.134 × 2	2.089 × 2	2.053 × 2	2.123 × 2

Table 3
The $B-O$ bond lengths in $A_2^{2+}B^{4+}O_4$ phases.

Phase	Sr_2FeO_4	Sr_2TiO_4	Sr_2VO_4
d_{B-O} (Å)	1.932 × 4	1.942 × 4	1.918 × 4
	1.950 × 2	1.915 × 2	1.985 × 2

Table 4
The $U-O$ bond lengths in A_2UO_4 phases.

Phase	K_2UO_4	Rb_2UO_4	Cs_2UO_4
d_{U-O} (Å)	2.168 × 4	2.172 × 4	2.190 × 4
	1.899 × 2	1.909 × 2	1.908 × 2

Cs_2UO_4 (1.914 Å) and $Cs_2U_2O_7$ (1.807 and 1.835 Å; Van den Berghe *et al.*, 2002) is in favour of our viewpoint, the idealized layers being more charged in the latter structure.

This model is also successfully applied to $R_{1+x}Sr_{2-x}Mn_2O_7$ (R = rare-earth; Mitchell *et al.*, 1997), second term of Ruddlesden–Popper structures. In these structures, the MnO_6 octahedron exhibits non-equivalent apical bonds, usually indicated by Mn—O1 and Mn—O2, with bond lengths of *ca* 1.94 and 2.03 Å, respectively. The layer sequence can be written here as –[A_RO2]–(MnO_2)–[A_PO1]–(MnO_2)–[A_RO2]–[A_RO2]–, where A_P refers to the A cation located inside the perovskite block and A_R to that of the rock-salt layer. If one assumes, as suggested by structural analyses, random distributions of the R^{3+} and Sr^{2+} cations over these sites, the formal charges of the layers will particularly lead to analogous displacements for the A_R and O2 ions as in K_2NiF_4 structures. On the other hand, the shortness of the Mn—O1 bond is associated with the location of the individual positive layer A_PO1 sandwiched between the negative MnO_2 ones. Moreover, the Mn—O2 bond length will be more sensitive to the doping. Actually, the slight shift of the Mn cation from the equatorial plane of its octahedron reflects the preferential occupancy of the A_P site by the rare-earth R^{3+} cations

The octahedral elongation can be controlled more easily and over a wide range by intercalating buffer positive layers between neutral adjacent rock-salt layers (AO)–(AO); hence, the tuning of the apical bond length can be achieved by varying the composition of the buffer layers and the size of the A cations, as realized in the Brownmillerites $A_2MnGaO_{5+\delta}$ (Abakumov, Rozova, Pavlyuk, Lobanov, Antipov, Lebedev, Tendeloo, Ignatchik, Ovtchenkov, Koksharov & Vasil'ev, 2001; Alekseeva *et al.*, 2004; Abakumov, Rozova, Pavlyuk, Lobanov, Antipov, Lebedev, Tendeloo, Sheptyakov, Balagurov & Bourée, 2001) and especially in the high-T_c cuprate superconductors, as shown below. For example, in $Sr_2MnGaO_{4.97}$, the Mn^{3+}—O apical bond lengths are enhanced to 2.41 Å (against 2.28 Å in $NdSrMnO_4$) using the deficient ($GaO_{0.97}$) buffer layer in the layer sequence –(MnO_2)–(SrO)–($GaO_{0.97}$)–(SrO)–(MnO_2)–.

The correlation of the physical properties with the magnitude of the octahedral elongations is well shown in the high-T_c cuprate superconductors, particularly for the related systems Bi–Sr–Ca–Cu–O, Tl–Ba–Ca–Cu–O and Hg–Ba–Ca–Cu–O, where it is established that the T_c increases from Bi to Hg (Putilin, Antipov, Chmaissem & Marezio, 1993; Putilin *et al.*, 1993; Schilling *et al.*, 1993) in structures containing the same number of perovskite layers. To analyse this evolution and understand its structural origin, we consider part of the stacking layers in such structures: –(CuO_2)–(SrO)–(BiO)–(BiO)–(SrO)–(CuO_2)–, –(CuO_2)–(BaO)–(TlO)–(TlO)–(BaO)–(CuO_2)– and –(CuO_2)–(BaO)–(Hg)–(BaO)–(CuO_2)– (Fig. 4); their formal charges are –(−2)–(0)–(+1)–(+1)–(0)–(−2)–, –(−2)–(0)–(+1)–(+1)–(0)–(−2)– and –(−2)–(0)–(+2)–(0)–(−2)–, respectively. Consequently, the resulting interlayer polarizations (in the undistorted configurations) are here more pronounced than in the Ruddlesden–Popper structures; the reason is related to the location of the neutral (Ba/SrO) layers between the buffer (Bi, Tl or Hg)O positive layers and the negative (CuO_2) ones. Indeed, as expected, the apical Cu—O bonds are more elongated here. Owing to the net charge of the buffer layers, this elongation is logically the maximum in Hg-based cuprates, even with the presence of some extra oxygen anions in this layer (Wagner *et al.*, 1993; Radaelli *et al.*, 1993). Moreover, because of the ionic radius, the effective positive charge density in the TlO layers is more pronounced than in the BiO ones, which leads to more elongated polyhedra in the Tl-based cuprates (Torardi *et al.*, 1988; Cox *et al.*, 1988). These strong elongations of the Cu—O apical bonds constitute an intrinsic doping of the corresponding Cu—O equatorial bonds, as shown by their consequent shortening: there is a partial transfer of electron density from the equatorial bonds to the apical bond. This doping is commonly associated with the overlapping of (Bi, Tl or Hg) 6*p* bands with the Fermi level. Both these opposite trends, *i.e.* the lengthening of the apical and the shortening of the equatorial bonds, increase T_c. However, both these bonds are shortened along with an extrinsic hole doping, as shown by $HgBa_2CaCu_2O_{6+\delta}$ (Radaelli *et al.*, 1993) with oxygen insertion, in correlation with the reduction of the net charge of the layers. The bell-shaped curve of T_c *versus* hole concentration (Presland *et al.*, 1991) is related to the competing effects of the contraction of apical and equatorial Cu—O bonds. At the beginning, the latter is predominant, which raises T_c; the subsequent rapid decrease of the apical bond length will reverse this tendency.

In the manganites colossal magnetoresistance was discovered in doped perovskites (Von Helmolt *et al.*, 1993), pyrochlores (Shimakawa *et al.*, 1996) and the n = 2 member of the Ruddlesden–Popper structures $La_{1+x}Sr_{2-x}Mn_2O_7$ (Moritomo *et al.*, 1996), but not in the n = 1 member

$La_{1-x}Sr_{1+x}MnO_4$, where a hole doping is carried out from the $LaSrMn^{3+}O_4$ compound. This is due to the net tetragonal elongation of the MnO_6 octahedra in this case, which prevents the transition from paramagnetic semiconductor to ferromagnetic metal, to be achieved by the temperature or magnetic field. However, when an electron doping is carried out from the $A_2^{2+}Mn^{4+}O_4$ compound, such as in $Ca_{2-x}La_xMnO_4$ (Maignan *et al.*, 1998), the weak octahedral elongation allows the above transition to be possible.

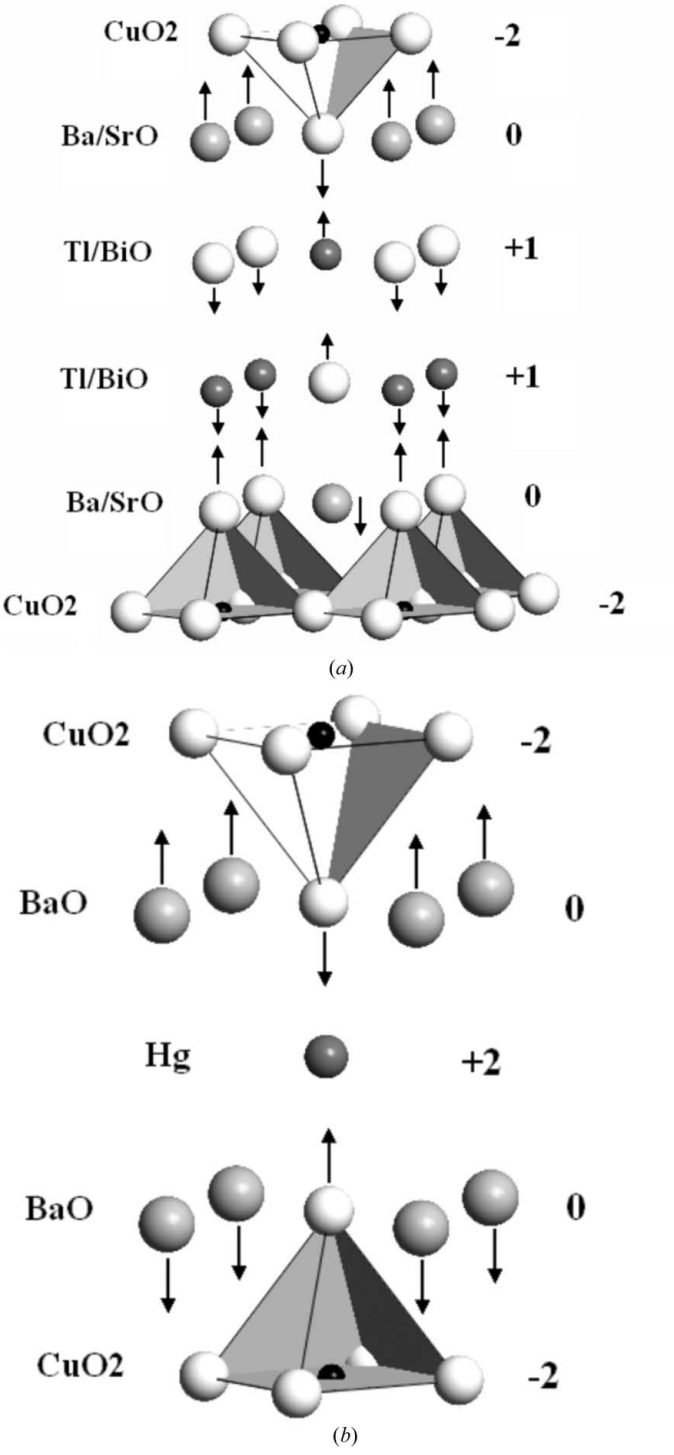

Figure 4
The formulae and the formal charges of the idealized layers and the ionic displacements in (*a*) $(Tl,Bi)_2(Ba,Sr)_2Ca_{n-1}Cu_nO_{2n+4+\delta}$ and (*b*) $HgBa_2Ca_{n-1}Cu_nO_{2n+2+\delta}$ (right).

4. Conclusions

The polyhedral distortions can be regarded in the same context as the consequences of a multi-scale minimization of the electric polarization. The magnitude and direction of the distortions are interpreted by invoking in the first step the formal charge and in the second step the distribution of valence-electron density. The results obtained by this approach are in good accordance with the structural data. In particular, the ferrodistortive order of JT distortions is obtained when the minimization deals with a formal charge interlayer polarization, while the antiferrodistortive one is adopted when only the valence-electron density is involved. The applications of this model for cuprate superconductors and manganites allow us to correlate the observed properties, the octahedral elongation and the structure–composition features.

A preliminary version of this work was presented at the International School on Mathematical and Theoretical Crystallography held in Nancy on 20–24 June 2005. I am grateful to Professor C. Lecomte for his help in facilitating my participation in this school.

References

Abakumov, A. M., Rozova, M. G., Pavlyuk, B. Ph., Lobanov, M. V., Antipov, E. V., Lebedev, O. I., Van Tendeloo, G., Ignatchik, O. L., Ovtchenkov, E. A., Koksharov, Yu. A. & Vasil'ev, A. N. (2001). *J. Solid State Chem.* **160**, 353–361.
Abakumov, A. M., Rozova, M. G., Pavlyuk, B. Ph., Lobanov, M. V., Antipov, E. V., Lebedev, O. I., Van Tendeloo, G., Sheptyakov, D. V., Balagurov, A. M. & Bourée, F. (2001). *J. Solid State Chem.* **158**, 100–111.
Alekseeva, A. M., Abakumov, A. M., Rozova, M. G., Antipov, E. V. & Hadermann, J. (2004). *J. Solid State Chem.* **177**, 731–738.
Bader, R. F. W. (1960). *Mol. Phys.* **3**, 137–151.
Bader, R. F. W. (1962). *Can. J. Chem.* **40**, 1164–1175.
Bader, R. F. W. (1990). *Atoms in Molecules – A Quantum Theory.* Oxford University Press.
Bader, R. F. W., Henneker, W. H. & Cade, P. E. (1967). *J. Chem. Phys.* **46**, 3341–3363.
Bednorz, J. G. & Muller, K. A. (1986). *Z. Phys. B*, **64**, 189–193.
Bersuker, I. B. (1996). *Electronic Structure and Properties of Transition Metal Compounds.* New York: Wiley.
Bersuker, I. B. (2005). *The Jahn–Teller Effect.* Cambridge University Press.
Bersuker, I. B. & Polinger, V. (1989). *Vibronic Interactions in Molecules and Crystals.* Berlin: Springer.
Birgeneau, R. J., Guggenheim, H. J. & Shirane, G. (1970). *Phys. Rev. B*, **1**, 2211–2230.
Bocquet, A. E., Fujimori, A., Mizokawa, T., Saitoh, T., Namatame, H., Suga, S., Kimizuka, N., Takeda, Y. & Takano, M. (1992). *Phys. Rev. B*, **45**, 1561–1570.
Britten, J. F., Dabkowska, H. A., Dabkowski, A. B., Greedan, J. E., Campbell, J. L. & Teesdale, W. J. (1995). *Acta Cryst.* C**51**, 1975–1977.
Cox, D. E., Torardi, C. C., Subramanian, M. A., Gopalakrishnan, J. & Sleight, A. W. (1988). *Phys. Rev. B*, **38**, 6624–6630.

Dai, P., Chakoumakos, B. C., Sun, G. F., Wong, K. W., Xin, Y. & Lu, D. F. (1995). *Physica C*, **243**, 201–206.
Dann, S. E., Weller, M. T. & Currie, D. B. (1991). *J. Solid State Chem.* **92**, 237–240.
Demazeau, G., Buffat, B., Pouchard, M. & Hagenmuller, P. (1984). *J. Solid State Chem.* **54**, 389–399.
Demazeau, G., Courbin, P., le Flem, G., Pouchard, M., Hagenmueller, P., Soubeyroux, J. L., Main, I. G. & Robins, G. A. (1979). *Nouv. J. Chim.* **3**, 171–174.
Devonshire, A. F. (1949). *Philos. Mag.* **40**, 1040–1063.
Devonshire, A. F. (1951). *Philos. Mag.* **42**, 1065–1079.
Devonshire, A. F. (1954). *Philos. Mag. Suppl.* **3**, 85–130.
Duribreux, I., Saadi, M., Obbade, S., Dion, C. & Abraham, F. (2003). *J. Solid State Chem.* **172**, 351–363.
Falvello, L. R. (1997). *J. Chem. Soc. Dalton Trans.* pp. 4463–4475.
Ganguly, P. & Rao, C. N. R. (1984). *J. Solid State Chem.* **53**, 193–216.
Geller, S. & Wood, A. E. (1956). *Acta Cryst.* **9**, 563–568.
Goodenough, J. B., Demazeau, G., Pouchard, M. & Hagenmuller, P. (1973). *J. Solid State Chem.* **8**, 325–330.
Grande, B. & Mueller-Buschbaum, H. (1977). *Z. Anorg. Allg. Chem.* **433**, 152–156.
Greedan, J. E. & Gong, W. (1992). *J. Alloys Compd.* **180**, 281–287.
Harrison, W. A. (1980). *Electronic Structure and the Properties of Solids.* San Francisco: W. H. Freeman & Co.
Hiroi, Z., Kobayashi, N. & Takano, M. (1996). *Physica C*, **266**, 191–202.
Jahn, H. A. & Teller, E. (1937). *Proc. R. Soc. Ser. A*, **161**, 220–235.
Kanamori, J. (1960). *J. Appl. Phys.* **31**, 14S–23S.
Kaplan, M. D. & Vekhter, B. G. (1995). *Cooperative Phenomena in Jahn–Teller Crystals. Series: Modern Inorganic Chemistry*. Berlin: Springer.
Khomskii, D. I. & Kugel, K. I. (1973). *Solid State Chem.* **13**, 763–766.
Kovba, L. M., Ippolitova, E. A., Simanov, Y. P. & Spitsyn, V. I. (1961). *Zh. Fiz. Khim.* **35**, 563–568.
Lecomte, C., Aubert, E., Legrand, V., Porcher, F., Pillet, S., Guillot, B. & Jelsch, C. (2005). *Z. Kristallogr.* **220**, 373–384.
Longo, J. M. & Raccah, P. M. (1973). *J. Solid State Chem.* **6**, 526–531.
Lufaso, M. W. & Woodward, P. M. (2004). *Acta Cryst.* B**60**, 10–20.
Lukaszewicz, K. (1959). *Rocz. Chem.* **33**, 239–242.
Maignan, A., Martin, C., Van Tendeloo, G., Hervieu, M. & Raveau, B. (1998). *J. Mater. Chem.* **8**, 2411–2416.
Mason, W. P. & Matthias, B. T. (1948). *Phys. Rev.* **74**, 1622–1636.
Mitchell, J. F., Argyriou, D. N., Potter, C. D., Jorgensen, J. D., Hinks, D. G. & Bader, S.D. (1997). *Mater. Res. Soc. Symp. Proc.* **453**, 343–348.
Moritomo, Y., Asamitsu, A., Kuwahara, H. & Tokura, Y. (1996). *Nature*, **380**, 141–144.
Nishijima, M., Takeda, Y., Inanishi, N., Yamamoto, O. & Kanno, R. (1991). *J. Jpn. Soc. Powder Metall.* **38**, 224–228.
Obbade, S., Dion, C., Bekaert, E., Yagoubi, S., Saadi, M. & Abraham, F. (2003). *J. Solid State Chem.* **172**, 305–318.
Pearson, R. G. (1983). *J. Mol. Struct. (Theochem.)*, **103**, 25–34.
Presland, M. R., Tallon, J. L., Buckley, R. G., Liu, R. S. & Flower, N. E. (1991). *Physica C*, **176**, 95–105.
Purcell, E. M. & Ramsey, N. F. (1950). *Phys. Rev.* **78**, 807.
Putilin, S. N., Antipov, E. V., Chmaissem, O. & Marezio, M. (1993). *Nature*, **362**, 226–228.
Putilin, S. N., Antipov, E. V. & Marezio, M. (1993). *Physica C*, **212**, 266–270.
Radaelli, P. G., Wagner, J. L., Hunter, B. A., Beno, M. A., Knapp, G. S., Jorgensen, J. D. & Hinks, D. G. (1993). *Physica C*, **216**, 29–35.
Rainwater, J. (1950). *Phys. Rev.* **79**, 432–434.
Range, K. J., Rau, F. & Klement, U. (1991). *Z. Naturforsch. Teil B*, **46**, 1315–1318.
Rao, C. N. R., Ganguly, P., Singh, K. K. & Mohan Ram, R. A. (1988). *J. Solid State Chem.* **72**, 14–23.
Reinen, D. (1979). *J. Solid State Chem.* **27**, 71–85.
Roth, R. S. (1957). *J. Res. Natl Bur. Stand.* **58**, 75–88.
Sander, K., Lehmann, U. & Mueller-Buschbaum, H. (1981). *Z. Anorg. Allg. Chem.* **480**, 153–156.
Schilling, A., Cantoni, M., Guo, J. D. & Ott, H. R. (1993). *Nature*, **363**, 56–58.
Shannon, R. D., Oswald, R. A., Parize, J. B., Chai, B. H. T., Byszewski, P., Pajaczowska, A. & Sobolewski, R. (1992). *J. Solid State Chem.* **98**, 90–98.
Shimakawa, Y., Kubo, Y. & Manako, T. (1996). *Nature*, **379**, 53–55.
Shirane, G., Pepinsky, R. & Frazer, B. C. (1956). *Acta Cryst.* **9**, 131–140.
Singh, K. K., Ganguly, P. & Goodenough, J. B. (1984). *J. Solid State Chem.* **52**, 254–273.
Slater, J. C. (1950). *Phys. Rev.* **78**, 748–761.
Soubeyroux, J. L., Courbin, P., Fournes, L., Fruchart, D. & le Flem, G. (1980). *J. Solid State Chem.* **31**, 313–320.
Sykora, R. E. & Albrecht-Schmitt, T. E. (2004). *J. Solid State Chem.* **177**, 3729–3734.
Takeda, Y., Imayoshi, K., Imanishi, N., Yamamoto, O. & Takano, M. (1994). *J. Mater. Chem.* **4**, 19–22.
Torardi, C. C., Subramanian, M. A., Calabrese, J. C., Gopalakrishnan, J., McCarron, E. M., Morrissey, K. J., Askew, T. R., Flippen, R. B., Chowdry, U. & Sleight, A. W. (1988). *Phys. Rev. B*, **38**, 225–231.
Tsirelson, V. G. & Ozerov, R. P. (1996). *Electron Density and Bonding in Crystals.* Bristol/Philadelphia: Institute of Physics.
Tsirelson, V. G. & Stash, A. (2004). *Acta Cryst.* A**60**, 418–426.
Van den Berghe, S., Verwerft, M., Laval, J.-P., Gaudreau, B., Allen, P. G. & Van Wyngardenz, A. (2002). *J. Solid State Chem.* **166**, 320–329.
Von Helmolt, R., Wecker, J., Holzapfel, B., Schultz, L. & Sanwer, K. (1993). *Phys. Rev. Lett.* **71**, 2331–2333.
Wagner, J. L., Radaelli, P. G., Hinks, D. G., Jorgensen, J. D., Mitchell, J. F., Dabrowski, B., Knapp, G. S. & Beno, M. A. (1993). *Physica C*, **210**, 447–454.
Whangbo, M.-H. & Koo, H.-J. (2002). *Solid State Sci.* **4**, 335–346.
Wheeler, R. A., Whangbo, M.-H., Hughbanks, T., Hoffmann, R., Burdett, J. K. & Albright, T. A. (1986). *J. Am. Chem. Soc.* **108**, 2222–2236.
Woodward, J. D., Almond, P. M. & Albrecht-Schmitt, T. E. (2004). *J. Solid State Chem.* **177**, 3971–3976.